BBA - Molecular Basis of Disease 1870 (2024) 167004

Contents lists available at ScienceDirect

BBA - Molecular Basis of Disease

journal homepage: www.elsevier.com/locate/bbadis

Unraveling the molecular mechanisms of cell migration impairment and apoptosis associated with steroid sulfatase deficiency: Implications for X-linked ichthyosis

Tae-Uk Kwon , Yeo-Jung Kwon , Hyoung-Seok Baek , Hyemin Park , Hyein Lee , Young-Jin Chun *

College of Pharmacy and Center for Metareceptome Research, Chung-Ang University, Seoul 06974, Republic of Korea

A B S T R A C T

Steroid sulfatase (STS) deficiency is responsible for X-linked ichthyosis (XLI), a genetic disorder characterized by rough and dry skin caused by excessive keratinization. The impaired keratinization process leads to reduced cell mobility and increased apoptosis, which can cause an excessive buildup of the stratum corneum. In this study, we investigated the mechanisms underlying XLI and found that STS deficiency reduces cell mobility and increases apoptosis in human keratinocyte HaCaT cells. To explore these mechanisms further, RNA-sequencing was conducted on skin tissues from STS transgenic and knockout mice. Our RNA-seq results revealed that STS deficiency plays a critical role in regulating multiple signaling pathways associated with cell mobility and apoptosis, such as Wnt/β signaling and the Hippo signaling pathway. Knockdown of the STS gene using shRNA in HaCaT cells led to an upregulation of E-cadherin expression and suppression of key factors involved in epithelial-mesenchymal transition (EMT), such as N-cadherin and vimentin. Inhibition of EMT involved the Hippo signaling pathway and reduction of HIF-1α. Interestingly, inhibiting STS with shRNA increased mitochondrial respiration levels, as demonstrated by the extracellular flux oxygen consumption rate. Additionally, we observed a significant increase in ROS production in partial STS knockout cells compared to control cells. Our study demonstrated that the excessive generation of ROS caused by STS deficiency induces the expression of Bax and Bak, leading to the release of cytochrome *c* and subsequent cell death. Consequently, STS deficiency impairs cell mobility and promotes apoptosis, offering insights into the pathophysiological processes and potential therapeutic targets for XLI.

1. Introduction

Steroid sulfatase (STS) mutations or deficiencies are the main cause of X-linked ichthyosis (XLI), which leads to excessive keratinization of the skin [1]. XLI is a genetic disease that primarily affects males, occurring with a frequency of 1 in 2000 to 6000 individuals [2,3]. In cases of STS deficiency, impaired cholesterol degradation results in the accumulation of cholesterol sulfate and improper shedding of keratinocytes, disrupting the turnover of the stratum corneum. The accumulation of lipids within the epidermis hampers the skin's barrier function and causes dry and scaly skin [4,5]. However, the precise mechanism underlying the excessive formation of the stratum corneum due to STS deficiency is not yet been fully understood. Therefore, these mechanisms must be elucidated to develop therapeutic approaches for XLI and excessive stratum corneum formation.

Some studies suggest that reduced keratinocyte mobility may contribute to the excessive formation of the stratum corneum [6,7]. Impaired cell mobility prevents keratinocytes from migrating effectively, leading to the accumulation of cornified cells on the skin surface [6,7]. Epithelial-mesenchymal transition (EMT), which involves the loss of cell-cell adhesion [8–10], has been widely studied due to its role in keratinization [8,11,12]. EMT is regulated by complex signaling pathways, including Wnt/β-catenin, HIF-1α, and the Hippo pathway [13–15]. Particularly, HIF-1α is closely associated with cellular respiration [16–18]. Previous studies have demonstrated that increased STS expression upregulates Twist1 and HIF-1α, inducing the Wnt/β-catenin pathway and EMT [19].

Cellular apoptosis also contributes to hypertrophy of the stratum corneum [20]. Widespread cell apoptosis disrupts the regular process of cornification, which contributes to the formation of the skin's physical barrier [21,22]. Normally, epidermal cell apoptosis occurs due to cell damage caused by ultraviolet B (UVB) radiation [8,22] and previous studies have demonstrated that keratinocytes exposed to UVB generate reactive oxygen species (ROS), thereby contributing to cell apoptosis [23,24]. Moreover, enhanced cellular respiration generates ROS [25,26], mitochondrial oxidative stress, and oxidative phosphorylation

Abbreviations: STS, Steroid sulfatase; EMT, Epithelial-mesenchymal transition; XLI, X-linked ichthyosis; HIF-1α, Hypoxia-inducible factor 1α; Lats1, Large tumor suppressor kinase 1; YAP1, Yes-associated protein 1; Bax, Bcl-2-associated X protein; Bak, Bcl-2 homologous antagonist/killer; Caspase 3, Cysteine-aspartic acid protease 3; TNF-α, Tumor necrosis factor α; OCR, Oxygen consumption rate; ROS, Reactive oxygen species; mtDNA, Mitochondrial DNA.

* Corresponding author.
E-mail address: yjchun@cau.ac.kr (Y.-J. Chun).

https://doi.org/10.1016/j.bbadis.2023.167004
Received 13 September 2023; Received in revised form 8 December 2023; Accepted 21 December 2023
Available online 3 January 2024

[27,28]. High ROS levels induce cell death by releasing cytochrome *c* from mitochondria and inducing key factors such as Bax and Bak, which promote cell apoptosis [29,30].

In this study, we investigated the molecular mechanisms underlying the excessive formation of the stratum corneum induced by STS deficiency. Particularly, we focused on exploring the relationship between STS expression levels and keratinocyte mobility, as well as cell death. To achieve this, we generated a novel mouse model with a specific exon 2 region deficiency in the X chromosome using the CRISPR/Cas9 system. Previous studies have utilized other STS-deficient mouse models [31], but they lacked specificity to the X chromosome, resulting in low reproducibility. Currently, XLI research heavily relies on patient samples, which only allows for limited analyses such as serum metabolite levels and gene expression patterns [32,33]. To overcome these limitations, we utilized our newly developed STS mouse model for RNA-seq analysis, which enabled the identification of enhanced or diminished signal transduction pathways such as cell mobility and cell apoptosis in STS deficiency. Collectively, our findings provide important insights into the mechanisms through which STS deficiency leads to excessive keratinization, thus establishing a scientific basis for the development of effective treatment strategies for XLI.

2. Materials and methods

2.1. Reagents

STX-64 was purchased from Santa Cruz Biotechnology (Santa Cruz, CA), TNF-α from Enzo Biochem (Farmingdale, NY), and TGF-β1 from Merck Millipore (Burlington, MA). All chemicals, except TNF-α, were prepared in dimethylsulfoxide (DMSO), stored as small aliquots at −20 °C, and then diluted as needed in cell culture media. DMEM was purchased from HyClone (Logan, UT). FBS and charcoal-stripped FBS were purchased from Tissue Culture Biologicals (Long Beach, CA). The Neon transfection system was obtained from ThermoFisher Scientific (Waltham, MA), and the D-Plus™ ECL solution was obtained from Dongin LS (Seoul, Korea). The following antibodies were used in our experiments: anti-STS polyclonal antibody (ab62219) from Abcam (Cambridge, MA), anti-vimentin (sc-6260), anti-HIF-1α (sc-13,515), anti-YAP1 (sc-101,199), anti-Bax (sc-7480), anti-Bak (sc-517,390), goat anti-rabbit IgG-Texas Red (sc-2780), and Ultra Cruz™ mounting medium (sc-24,941) from Santa Cruz Biotechnology (Santa Cruz, CA), anti-E-cadherin (07–697) from Merck Millipore (Burlington, MA), anti-N-cadherin (4061S), anti-phospho-YAP1 (4911S), anti-Lats1 (3477S), anti-phospho-Lats1 (9157S), anti-caspase 3 (9662S), and anti-cleaved caspase 3 (9662S) from Cell Signaling Technology (Danvers, MA), and anti-GAPDH from Cusabio Technology (Houston, TX). All other chemicals were obtained from commercial sources.

2.2. Cell culture

The HaCaT human keratinocyte cell line was obtained from CLS Cell Lines Service (Germany). HaCaT, pLjm1-Control HaCaT, and pLjm1-STS HaCaT cell lines were cultured in Dulbecco's Modified Eagle Medium (DMEM) supplemented with 10 % (*v*/v) fetal bovine serum (FBS), 100 U/mL penicillin, and 100 μg/mL streptomycin. Cas9-HaCaT and Cas9-STS$^{+/-}$ HaCaT cell lines were cultured in DMEM supplemented with 20 % (*v*/v) FBS, 100 U/mL penicillin, and 100 μg/mL streptomycin. All cell lines were incubated at 37 °C in a humidified atmosphere with 5 % CO_2. After 24 h of incubation, the cells were treated with TNF-α or STX-64 for 24 or 48 h.

2.3. Transient and stable transfection

For transient transfections, the STS coding sequence was cloned into the pcDNA3.1/Zeo^{+} vector. The cells were transfected with 40 nM siRNA or 3 μg plasmid using the Neon Transfection System (Life Technologies, CA). The plasmid vectors pLJM1-Empty (a gift from Joshua Mendell, Addgene plasmid # 91980), pLKO.1 puro (a gift from Bob Weinberg, Addgene plasmid #8453), pMD2.G, and psPAX2 (gifts from Didier Trono, Addgene plasmids # 12259 and #12260) were obtained from Addgene [34,35]. HEK293T cells were co-transfected with the pLJM1-STS, pMD2.G, and psPAX2 vectors. After 48 h, the lentiviral supernatant containing the STS gene was collected and used to treat HaCaT cells along with polybrene (8 μg/mL) for 24 h. HaCaT cells overexpressing STS were selected using puromycin (1 μg/mL). The optimal sequence of siRNAs targeting human STS was cloned into the pLKO.1 plasmid, which encodes a lentiviral vector containing a multiple cloning site for the insertion of shRNA constructs driven by an upstream U6 promoter. The modified plasmid or empty vector was further co-transfected into HEK293T cells with lentiviral packaging plasmids to generate STS or control shRNA lentivirus. HaCaT cells were infected with the constructed control and STS shRNA lentivirus for 24 h, and infected cells were selected using puromycin treatment. After 24 h, the media was replaced with puromycin-free growth media, and the cells were cultured for further STS knockdown studies.

2.4. Generation of Cas9-STS$^{+/-}$ HaCaT cells

The plasmid vectors pLentiCas9-T2A-GFP (a gift from Roderic Guigo & Rory Johnson, Addgene plasmid # 78548) and tet-pLKO-sgRNA-puro (a gift from Nathanael Gray, Addgene plasmid # 104321) were obtained from Addgene [35]. Lentiviral supernatants containing the Cas9 gene or STS sgRNA were prepared using HEK293T cells. Cas9-STS$^{+/-}$ HaCaT cells were isolated by single-cell separation using 96-well plates.

2.5. Quantitative PCR (qPCR)

qPCR analysis was performed using a Rotor-Gene Q machine (Qiagen, Netherlands) and analyzed with the QIAGEN Rotor-Gene Q Series software. Each reaction consisted of 10 μL of Q Green 2× qPCR Master Mix, 1 μM of oligonucleotide primers, and 20 ng of cDNA in a final volume of 20 μL. The amplification program included one cycle at 95 °C for 5 min, followed by 40 cycles of denaturation at 95 °C for 15 s, and annealing/extension at 56 °C for 45 s. The following primer sets were used for qPCR: STS, 5′- CCT CCT ACT GTT CTT TCT GTG GG-3′ (forward) and 5′-TGC CAG TIT CTG CAT CTG C-3′ (reverse); E-cadherin, 5′- GTA CTT GTA ATG ACA CAT CTC-3′ and 5′- GGT CGA TAT TGG GAG TCC TGA TA-3′; 18S rRNA, 5′-GTA ACC CGT TGA ACC CCA TT-3′ and 5′-CCA TCC AAT CGG TAG TAG CG-3′; N-cadherin, 5′-GGT GGA GGA GAA GAA GAC CAG-3′ and 5′- GGC ATC AGG CTC CAC AGT −3′; Vimentin, 5′- CCA AAC TTT TCC TCC CTG AAC C-3′ and 5′- GTG ATG CTG AGA AGT TTC GTT GA-3′; E-cadherin (mouse), 5′- CAG TTC CGA GGT CTA CAC CTT-3′ and 5′- TGA ATC GGG AGT CTT CCG AAA A-3′; N-cadherin (mouse), 5′-CTC CAA CGG GCA TCT TCA TTA T-3′ and 5′- CAA GTG AAA CCG GGC TAT CAG-3′; Vimentin (mouse), 5′- CGT CCA CAC GCA CCT ACA G-3′ and 5′- GGG GGA TGA GGA ATA GAG GCT-3′; GAPDH (mouse), 5′-TGG ATT TGG ACG CAT TGG TC-3′ and 5′-TTT GCA CTG GTA CGT GTT GAT-3′.

2.6. Luciferase reporter assay

For transfection, the cells were seeded at a density of 1.5×10^4/well and transfected with GLUT-1 or E-cadherin reporter plasmids using the Neon™ transfection system (Invitrogen) according to the manufacturer's instructions. pRL-Renilla (Promega, Madison, WI) was co-transfected as a control. After 24 h, the cells were lysed using lysis buffer and luciferase activities were measured with a FilterMax F3 microplate reader (Molecular Devices) using the Dual-Luciferase® Reporter system (Promega).

2.7. Western blotting analysis

Cells and mouse skin samples were lysed using ice-cold PE buffer containing 50 mM NaF. Protein lysates were separated by SDS-PAGE on 8 % or 12 % polyacrylamide gels and electrophoretically transferred to 0.45 μm PVDF membranes. The membranes were blocked with 5 % (*w/v*) BSA in Tris-buffered saline containing 0.1 % Tween-20 (TBST) for 2 h at 4 °C, incubated with primary antibodies diluted at a 1:1000 ratio in TBST, and then incubated with secondary antibodies for 2 h. Protein bands were visualized using D-Plus™ ECL solution (Dongin LS, Korea) and analyzed with a ChemiDoc XRS (Bio-Rad, CA).

2.8. Cell viability assay

Cells were seeded in 96-well plates at a density of 5×10^4 cells/well and incubated for 1–6 days. For the treatment experiments, the cells were treated with 10 μM STX-64 and incubated for 48 h. EZ-CyTox solution (DoGenBio, Korea) was added to each well, and cell viability was measured after a 2-h incubation period at a wavelength of 450 nm using a Sunrise™ microplate reader (Tecan, Männedorf, Switzerland).

2.9. Cell cycle assay

Cells were collected using 0.1 % trypsin-EDTA, washed twice with PBS, and suspended in 70 % cold ethanol. After fixation, the cells were washed twice with PBS and stained with the Muse™ Cell Cycle Assay kit (Merck Millipore, Germany). Analysis of the cell cycles was performed using the Muse™ cell analyzer (Merck Millipore, Germany).

2.10. Immunofluorescence

Samples were fixed with 10 % neutral formalin for 30 min at 24 °C, blocked for 45 min in PBS buffer containing 10 % goat serum and 0.2 % Triton X-100, incubated with a primary antibody (1:200) overnight at 4 °C, and then stained with goat anti-rabbit IgG-Texas Red (1:200) overnight. After three PBS washes, coverslips were mounted onto glass slides using Ultra Cruz™ mounting medium. Fluorescence was then analyzed using an LSM 800 confocal laser scanning microscope (Carl Zeiss, Germany).

2.11. Scratch wound assay

The cells were seeded at a density of 1×10^6 cells/well in 6-well plates and allowed to adhere for 24 h. The cells were then treated with mitomycin C (25 μg/mL) for 30 min, washed with PBS, and a scratch wound was created using a sterile pipette tip. The cells were allowed to migrate for 48 h, and images of the wound were captured at predetermined time points using an inverted microscope.

2.12. Invasion assay

Cancer cell invasion was examined using the QCM™ 24-well Cell Invasion Assay Kit (Millipore), according to the manufacturer's protocol. Briefly, 300 μL of cell suspension in serum free media (1×10^6 cells/mL) were seeded onto insert chambers with an 8 μm collagen-coated polycarbonate membrane. The ECM layer-invaded cells were stained with DAPI. Invading cells were visualized and observed under an LSM 800 confocal laser scanning microscope (Carl Zeiss, Germany) for counting of cell numbers. Each experiment was repeated at least ten times.

2.13. Measurement of oxygen consumption rate (OCR)

OCR was measured using the Seahorse XFe24 extracellular flux analyzer (Agilent Technologies, USA) according to the manufacturer's instructions. The cells were inoculated into Seahorse XFe 24-well plates approximately 24 h prior to the experiment, following the Seahorse protocol. The ideal density of 2000 cells per well was determined after the initial experiment. On the day of the experiment, sensor columns were hydrated in XF calibration solution and maintained at 37 °C in air without CO_2. The cells were then washed and incubated with a bicarbonate-free, low-buffer assay medium for 1 h at 37 °C. Afterward, the cells were incubated for 1 h at 37 °C and OCR changes were regularly monitored throughout the mitochondrial function assay. OCR was measured with a serial injection of oligomycin (1 μM), FCCP (1 μM), antimycin (0.5 μM), and rotenone (0.5 μM).

2.14. ROS generation

Cells were harvested, washed, and suspended in PBS containing 1 mM DCFH-DA. After incubation at 37 °C for 30 min, the cells were collected and resuspended in PBS. The level of ROS was determined by measuring the fluorescence intensity using a Sunrise™ microplate reader (Tecan) with an excitation wavelength of 480 nm and an emission wavelength of 520 nm.

2.15. Chromatin immunoprecipitation (ChIP)

ChIP assays were performed using the EZ ChIP™ Chromatin Immunoprecipitation Kit (Millipore, USA) following the manufacturer's instructions. HaCaT cells were treated with 4 % PFA for 15 min to cross-link the chromatin, after which the samples were sonicated to shear the DNA into 500-bp fragments. Immunoprecipitation was carried out for 6 h using anti-Twist1 or c-Myc antibodies and control IgG antibody, followed by the addition of 30 μl of magnetic beads. The collected precipitated chromatin was subjected to RT-qPCR analysis. The following primers were used for PCR: Twist1 protein binding site, 5′-GAA CCC AAG AGG CGA AGG-3′ (forward) and 5′-GGT GCT GGA CAT TGA AGA TTA CT-3′ (reverse); c-Myc protein binding site, 5′-GCC AGG ATG GTC TCA ATC TC-3′ (forward) and 5′-CTC CCT ATG CTG TTG TGG G-3′ (reverse).

2.16. Generation of STS transgenic (TG) mouse and STS KO mouse

A 7088-bp fragment of the human STS gene containing the CMV promoter was synthesized and cloned into the Amp^R site of the pcDNA3.1 vector to generate the STS plasmid for microinjection. The *Pvu*I and *Avr*II restriction enzymes were used to remove the 4.4-kb backbone fragment through gel extraction, leaving a 2.2-kb fragment. STS transgenic mice (C57BL/6 J) were generated by microinjecting the STS DNA into the male pronucleus of zygotes and transferring the embryos into the oviducts of pseudopregnant recipient female mice. Once the F_0 generation was born, genotyping tests were performed using tail cut samples to confirm the presence of the STS gene by PCR analysis with a forward primer for the CMV promoter and a reverse primer for the human STS gene. The Cas9 targeting vector is designed to contain gRNAs targeting the Cas9 gene to induce double-strand breaks (DSBs) in the gene of interest. The vector also contains a selection cassette, such as puromycin resistance genes, to select successfully targeted cells. The Cas9 targeting vector was introduced into ES cells using PEG-mediated transfection. The cells were then cultured under puromycin selection to select for cells that had incorporated the targeting vector. PCR and Southern blot analysis were conducted to screen for successful targeting events in the ES cells. PCR primers were designed to amplify the region flanking the Cas9 gene and the targeting vector, whereas Southern blot probes were designed to hybridize to specific regions within the Cas9 gene. Successfully targeted ES cells were injected into blastocysts and transferred into pseudopregnant females to generate chimeric mice (C57BL/6 N). Chimeric mice are composed of a mixture of cells from the original blastocyst and the injected ES cells. All animal experiments were approved by the Institutional Animal Care and Use Committee of the University of Chung-Ang and the STS transgenic mice were

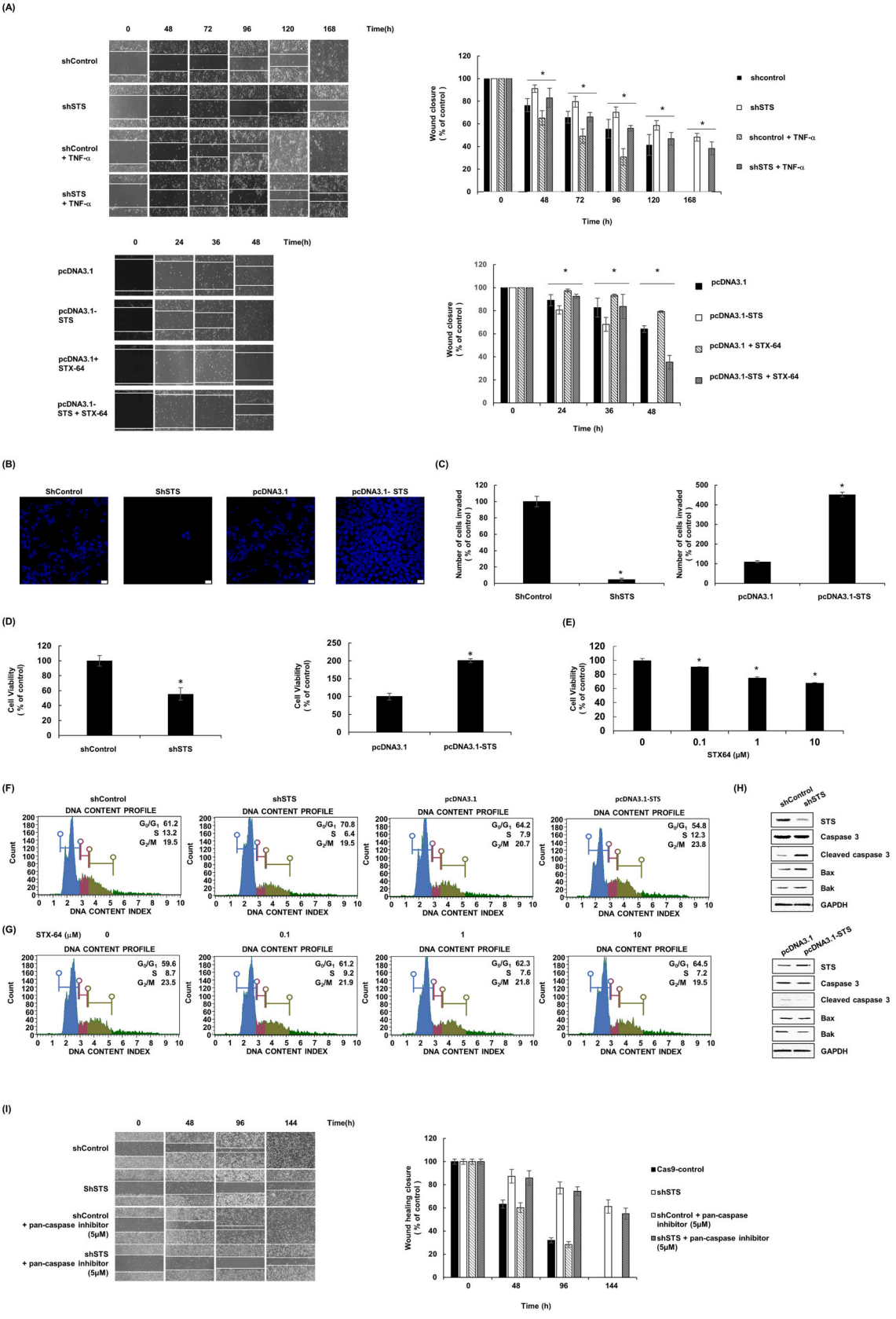

(caption on next page)

Fig. 1. Down-regulation of STS reduces cell mobility and induces cell apoptosis in human keratinocyte cells. (A) Images of the scratch wound assay. The data represent the mean ± SD ($n = 3$), $^*p < 0.05$. shSTS-HaCaT cells were treated with TNF-α (100 ng/ml) for 24 h. An injury line was created, and plates were photographed from 0 to 168 h. HaCaT cells were transfected with pcDNA3.1-STS and treated with STX-64 (10 μM) for 24 h. An injury line was created, and plates were photographed from 0 to 48 h. (B, C) Cell invasion was measured using the transwell invasion assay in the shSTS and pcDNA3.1-STS HaCaT cells. Data were from 10 independently quantified experiments. (B) The number of invading cells were plotted and the confocal microscopic analysis for invaded cells were conducted using DAPI staining, and (C) the number of invading shcontrol or pcDNA3.1-control cells was compared to the number of invading shSTS or pcDNA3.1-STS cells and the relative percentage of cell invasion. The data represent the mean ± SD ($n = 10$), $^*p < 0.05$. (D, E) Cell viability was measured using the CCK assay. The data represent the mean ± SD (n = 3). Cells were seeded at 1×10^5 cells/well in a 96-well plate and incubated for 24 h. (D) shSTS-HaCaT and pcDNA3.1-STS HaCaT were used. (E) HaCaT cells were treated with STX-64 (0, 0.1, 1, 10 μM) for 24 h. (F, G) The cell cycle was measured using a Muse cell cycle kit. The data represent the mean ± SD (n = 3); $^*p < 0.05$. The cells were seeded at 5×10^5 cells/well in a 12-well plate and incubated for 24 h. (F) shSTS-HaCaT and pcDNA3.1-STS HaCaT were used. (G) HaCaT cells were treated with STX-64 (0, 0.1, 1, 10 μM) for 24 h. (H) Total cellular protein (20 μg) in shSTS-HaCaT or pcDNA3.1-STS HaCaT cells was subjected to western blot analysis with caspase 3-, cleaved caspase 3-, Bax-, and Bak-specific antibodies. GAPDH was used as a loading control. (I) Images of the scratch wound assay. The data represent the mean ± SD (n = 3), $^*p < 0.05$. shSTS-HaCaT cells were treated with a pan-caspase inhibitor (5 μM) for 24 h. An injury line was created, and plates were photographed from 0 to 144 h.

maintained in pathogen-free conditions at Macrogen, Inc. (Seoul, Korea).

2.17. RNA-sequencing

Skin tissue samples from 8-week-old male mice were used. Total RNA was used to prepare libraries with the NEB Next Ultra II Directional RNA-Seq Kit (New England Biolabs, UK). Poly(A) RNA was isolated using the Poly(A) RNA Selection Kit (Lexogen, Austria), and the resulting mRNA was used for cDNA synthesis and shearing according to the manufacturer's instructions. Illumina indexes 1–12 was used for indexing, and PCR was performed for enrichment. Fragment sizes were evaluated using the Agilent 2100 bioanalyzer with the DNA High Sensitivity Kit, and library quantification was performed using the library quantification kit and a Step One Real-Time PCR System (Life Technologies, CA). High-throughput paired-end 100 sequencing was conducted using a HiSeq X10 sequencer (Illumina, CA).

2.18. Immunohistochemistry staining

Mouse tissues were fixed in formalin for at least three days, processed, and embedded in paraffin. Four-micron sections were cut, baked at 60 °C for at least 30 min, and cooled. The sections were then deparaffinized in three changes of xylene for 5 min each and rehydrated using an alcohol and distilled water gradient. If necessary, heat-induced epitope retrieval (HIER) was performed by steaming the slides for 20 min, cooling them for 20 min, and transferring them into wash buffer for 5 min. Citrate buffer at pH 6.0, Tris-EDTA buffer at pH 9.0, or Trilogy was used as the antigen retrieval buffer. The slides were transferred to TBS-Tween (TBS-T) wash buffer (0.05 M Tris, 0.15 M NaCl, 0.05 % Tween-20, pH 7.6) for 5 min, then loaded onto a Dako Autostainer Plus automated immunohistochemistry (IHC) system. Antibodies were diluted in TBS containing 1 % BSA at pH 7.5. Endogenous peroxidase was blocked with a 3 % hydrogen peroxide solution for 8 min. When using the biotinylated goat anti-mouse secondary antibody, 15 % normal goat serum in TBS with 1 % BSA was used for 10 min as the protein block. To develop the signal, two sequential applications of 3,3′-diaminobenzidine were used for 4 min each, followed by a 2-min incubation of hematoxylin as the counterstain. After staining, the slides were dehydrated via an alcohol gradient, cleared in xylene, and coverslipped.

2.19. Transcriptome analysis

Mouse skin samples were sequenced using a standard Illumina protocol (Shanghai Bingwang Biotechnology Co., Ltd.). The reads were mapped to the mouse genome (Mm9) using HISAT2 (v2.1). Gene counts were estimated using HTSeq. Differential expression analysis was performed using the 'DESeq2' R package. Genes with a fold-change >2 and an adjusted p-value <0.05 were defined as differentially expressed genes (DEGs). GO enrichment analysis of the DEGs was performed using the 'topGO' R package. GSEA was conducted according to the GSEA manual [36].

2.20. Statistical analysis

Dunnett's pairwise multiple comparison t-test was performed using GraphPad Prism 7 software (GraphPad Software, CA). Differences were considered statistically significant at $^*p < 0.05$.

3. Results

3.1. STS insufficiency impairs cell mobility and induces cell apoptosis in human keratinocytes

Thickening of the stratum corneum can be attributed to reduced cell migration and increased apoptosis. To investigate the effect of STS inhibition on cell mobility, shRNA was used to knock down STS expression in human keratinocyte HaCaT cells, after which we measured wound closure in the presence or absence of TNF-α, an STS inducer (Fig. 1A) [37,38]. The control cells achieved complete wound closure, whereas STS knockdown cells took >168 h to close the wound. However, when control cells were treated with TNF-α (100 ng/ml), wound closure was achieved 48 h earlier. Additionally, TNF-α also enhanced wound closure in STS knockdown cells at 168 h. Similar results were obtained when STS expression was downregulated using siRNA (Fig. S1A). Conversely, transient overexpression of STS significantly shortened the time for wound closure by 48 h, and STX-64, an irreversible STS inhibitor [39], inhibited STS-mediated cell mobility (Fig. 1A). Based on these results, we investigated cell invasion following STS deficiency. We found that STS deficiency strongly inhibited cell invasion by >90 %. In contrast, overexpression of STS increased cell invasion by 4.5-fold (Fig. 1B, C). These findings demonstrate that downregulation of STS expression or activity using shRNA or a specific inhibitor inhibits human keratinocyte migration and invasion.

Furthermore, we assessed cellular apoptosis levels in HaCaT cells based on STS regulation. STS inhibition by shRNA reduced cell viability, whereas transient overexpression of STS increased cell viability (Fig. 1D). Treatment with STX-64 at varying concentrations (0, 0.1, 1, or 10 μM) resulted in a concentration-dependent decrease in cell viability (Fig. 1E). Cell cycle analysis showed that STS downregulation by shRNA increased the proportion of cells in the G_0/G_1 phase (Fig. 1F). Similarly, treatment with STX-64 led to an increased proportion of cells in the G_0/G_1 phase compared to the control treatment (Fig. 1G). Additionally, STS deficiency by shRNA inhibited cell proliferation and promoted keratinocyte differentiation (Fig. S1B-G). Since previous studies have reported that keratinocytes undergo apoptosis during G_0/G_1 cell cycle arrest [40,41], we examined the levels of apoptotic factors, including caspase 3, Bax, and Bak, to confirm the increase in apoptosis following STS knockdown (Fig. 1H). Here, we observed elevated cleavage of caspase-3 and increased expression of Bax and Bak in shSTS-transfected cells, indicating that suppression of STS induced cellular apoptosis.

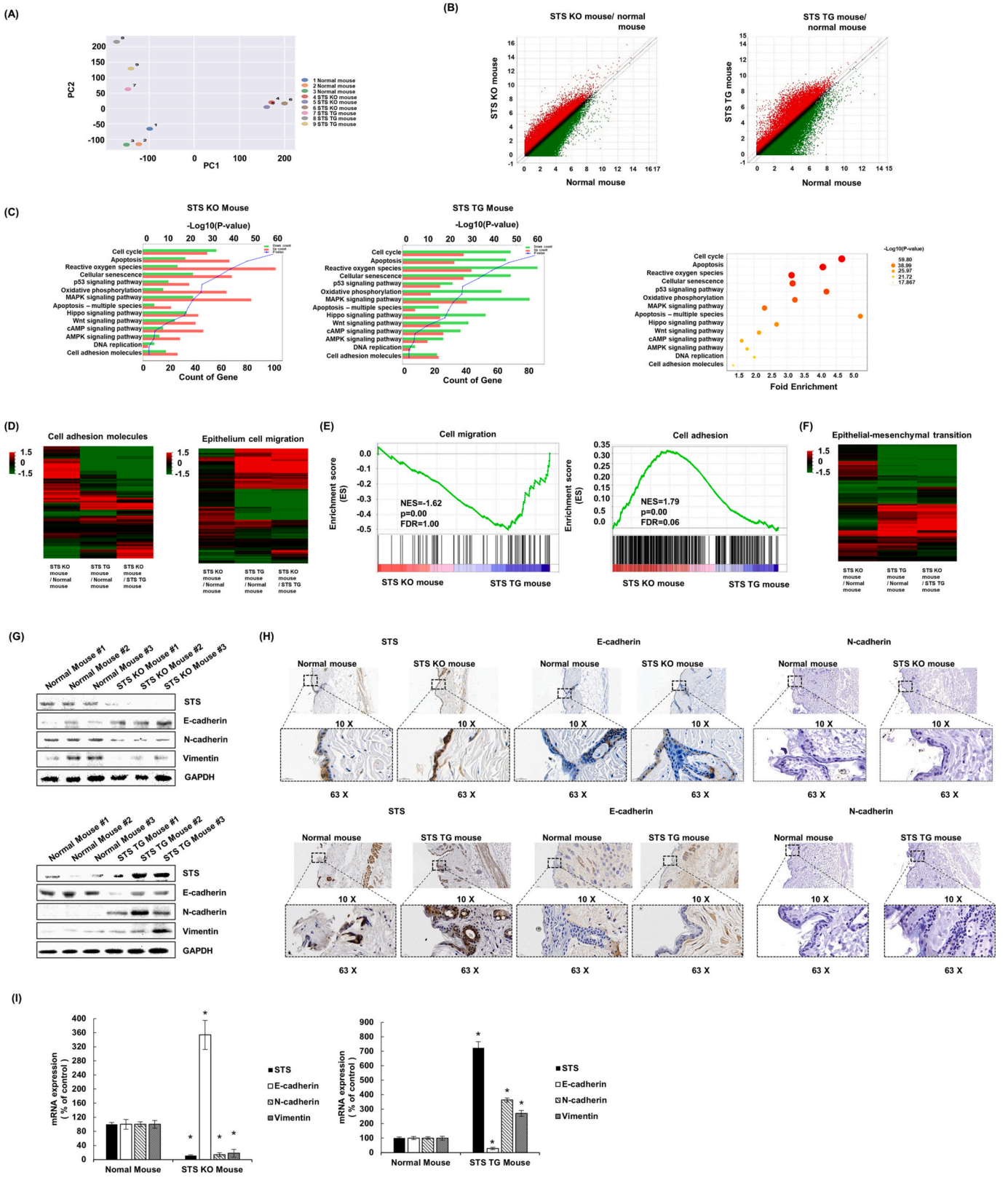

(caption on next page)

Fig. 2. Effects of STS gene deficiency of gene expression in mouse skin. PCA analysis, scatter plot, heat map, and GSEA analysis of RNA-seq expression in STS KO, STS TG, and normal mouse skin. (A) PCA analysis of STS KO, STS TG, and normal mouse. (B) Scatter plot of differentially expressed genes (DEGs) of upregulated (red) and downregulated (green) gene clusters in STS KO mouse skin vs. normal mouse skin or STS TG mouse vs. normal mouse skin. The fold threshold line is set at 1.5. (C) Gene ontology analysis of downregulated (green) and upregulated (red) gene clusters in STS KO and TG mouse skin. (D, E) Heatmap analysis of differentially expressed genes in each comparison group, with expression adjusted and normalized on a $\log_2$ scale. Red indicates upregulation, green indicates downregulation. (D) Heatmaps of cell adhesion molecules and epithelial cell migration in STS KO, STS TG, and normal mouse skin. (E) Cell adhesion molecules and epithelial cell migration pathways significantly enriched in STS KO and STS TG mouse skin based on GSEA analysis. (F) Heatmaps of epithelial-mesenchymal transition in STS KO, STS TG, and normal mouse skin. (G) Total protein (40 μg) from the skin of STS KO and STS TG mice subjected to western blot analysis with E-cadherin, N-cadherin, and vimentin antibodies. GAPDH was used as a loading control. (H) Immunohistochemistry (IHC) staining was performed on the skin of STS KO and STS TG mice using STS, E-cadherin, and N-cadherin antibodies. Each data point represents the mean ± SEM of three experiments. $^*p < 0.05$ compared to control. (I) Real-time qPCR to detect the expression of E-cadherin, N-cadherin, and vimentin mRNA in STS KO and STS TG mouse skin. Each data point represents the mean ± SEM of three experiments. $^*p < 0.05$ compared to control. (For interpretation of the references to colour in this figure legend, the reader is referred to the web version of this article.)

Conversely, STS overexpression decreased the levels of cleaved caspase 3, Bax, and Bak expression. Therefore, our findings suggest that STS deficiency in keratinocytes decreases cell migration and increases apoptosis. Also, pan-caspase inhibitor to inhibit apoptosis did not alter cell mobility (Fig. 1I). Thus, the reduction in cell motility and the induction of apoptosis due to STS deficiency may be independent processes.

3.2. STS deficiency in mice and HaCaT cells regulates the gene expression levels of EMT-related factors to suppress the EMT process.

To further investigate the role of STS in stratum corneum formation, we generated new STS knockout (KO) and transgenic (TG) mouse models and conducted RNA-seq analysis using skin tissues from these mice (8-week-old male). Principal components analysis (PCA) of quantitative data for the expression levels of approximately 39,000 genes indicated distinct populations for STS KO, STS TG, and normal mice, respectively (Fig. 2A). The gene expression distribution for each mouse was visualized using scatter plots with a 1.5-fold threshold line (Fig. 2B). Ontology analysis demonstrated significant alterations in genes involved in cellular processes, including apoptosis, based on STS levels in mice (Fig. 2C). Notably, genes associated with apoptosis, reactive oxygen species, oxidative phosphorylation, and various other signaling pathways, including the Hippo pathway, were significantly upregulated in STS KO mice, whereas they were significantly downregulated in STS TG mice (Fig. 2C). Furthermore, we explored the potential correlation between STS insufficiency and inhibition of cell motility through differential gene expression analysis. To achieve this, we utilized the Mouse Genome Informatics (MGI) database (https://www.informatics.jax.org/) to select candidate cell adhesion molecules and factors for epithelial cell migration from the RNA-seq data (Supplementary Data Table S1) and generated gene heatmaps using the selected gene list (Fig. 2D). As illustrated in the heatmaps in Fig. 2D, the expression levels of cell adhesion molecules were increased, whereas factors associated with epithelial cell migration were suppressed in response to STS deficiency. Gene set enrichment analysis (GSEA) further confirmed the induction of cell adhesion molecules and inhibition of epithelial cell migration-related factors in STS KO mice compared to STS TG mice (Fig. 2E). Collectively, our findings revealed that STS insufficiency in mice significantly inhibited the expression of EMT markers and induced cell adhesion molecules associated with cell mobility, as summarized in Fig. 2F. Additionally, we determined the protein expression levels of EMT-related factors in STS KO and TG mice. E-cadherin, a well-known marker for the mesenchymal-epithelial transition (MET) process, was strongly enhanced in STS KO mice, while EMT markers such as N-cadherin and vimentin were markedly downregulated (Fig. 2G-I). Conversely, STS TG mice exhibited suppression of E-cadherin expression along with a marked induction of N-cadherin and vimentin (Fig. 2G-I).

Furthermore, we examined the expression levels of EMT-related factors in HaCaT cells to investigate whether STS deficiency also inhibits the EMT process. As a marker of MET, E-cadherin was significantly increased, whereas N-cadherin and vimentin were strongly reduced in the context of STS deficiency (Fig. 3A-F) [8]. Conversely, STS overexpression notably hindered E-cadherin expression and elevated the levels of N-cadherin and vimentin. Interestingly, the knockdown of STS significantly increased the promoter activity of E-cadherin by approximately 2.5-fold, whereas STS overexpressing cells exhibited a 20 % reduction in E-cadherin promoter activity (Fig. 3H). Given that we found that STS also regulates EMT-inducing transcription factors that suppress E-cadherin (Fig. S2F), we further investigated the key regulator responsible for E-cadherin suppression by STS. Surprisingly, the results of our ChIP assays demonstrated that Twist1, which is known as a master regulator of cell migration and metastasis [42], and c-Myc, which is known to promote EMT together with Twist1 [42–44], both bind to the promoter site of E-cadherin. The level of binding was significantly reduced in STS knocked-down cells, indicating that the suppression of E-cadherin transcription by Twist1 and c-Myc was alleviated by STS deficiency (Fig. 3I). However, overexpression of STS yielded opposite results. Additionally, restoration of EMT, which was reduced upon STS deficiency, increased cell mobility (Fig. S2G, H).

Collectively, our findings demonstrate that STS deficiency in cells and mice inhibits the EMT process through the modulation of EMT-related factors. Specifically, we observed the transcriptional regulation of E-cadherin by Twist1 and c-Myc, which directly bind to the promoter region of E-cadherin.

3.3. STS deficiency may impede the EMT process through the activation of the Hippo pathway and suppression of HIF-1α expression

To investigate the detailed molecular mechanisms underlying EMT inhibition in STS-deficient conditions, we examined the protein levels of key factors in the Hippo signaling pathway, including Lats1, YAP1, and HIF-1α, which we found to be induced by STS through the activation of the Wnt/β -catenin signaling pathway in our previous study [19]. Intriguingly, inhibition of STS activity by shRNA or STX-64 significantly increased the protein levels of Lats1, pLats1, and pYAP1, while downregulating YAP1, indicating that STS insufficiency activates the Hippo signaling pathway. Conversely, STS overexpression or TNF-α treatment yielded opposite results (Fig. 4A-C). These results suggest that STS insufficiency may suppress the expression of EMT-related factors through the activation of Hippo signaling.

As illustrated in Fig. 2C, Wnt/β-catenin signaling was inhibited in STS knockout (KO) mice. Therefore, we next investigated whether HIF-1α expression was decreased in STS-downregulated human keratinocytes. Surprisingly, STS suppression markedly decreased the protein level of HIF-1α, whereas STS induction significantly elevated HIF-1α expression in cells (Fig. 4D, E). Furthermore, the gene expression levels of several prolyl hydroxylases (PHD) including P4HA2 and P4HB, which are known to induce the phosphorylation of HIF-1α [16–18], were significantly increased in STS KO mice according to our RNA-seq data (Fig. 4F). The induction of PHDs in response to STS deficiency may hinder HIF-1α expression by enhancing phosphorylation and protein degradation. These findings indicate that the inhibition of the EMT process in STS-insufficient conditions may occur through the activation

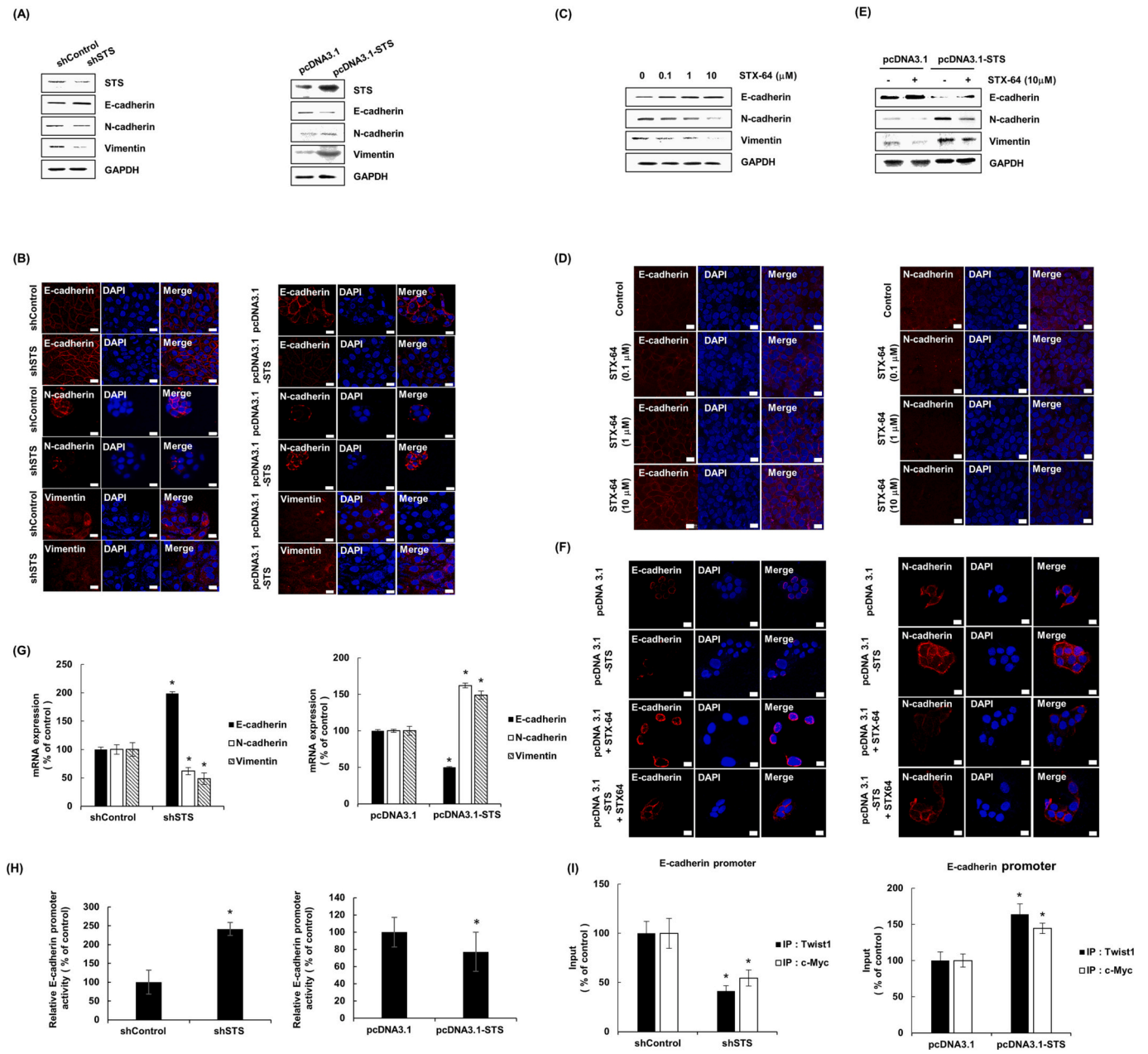

Fig. 3. STS suppresses EMT makers such as N-cadherin and vimentin in HaCaT cells. (A, C, E) Total cellular protein (20 μg) was subjected to western blot analysis using STS, E-cadherin, N-cadherin, and vimentin antibodies. GAPDH was used as a loading control. (B, D, F) Immunofluorescence staining. Cells were fixed, incubated with E-cadherin, N-cadherin, and vimentin antibodies, stained with Alexa Fluor 594-labeled secondary antibody, and imaged using fluorescence microscopy. Microscopy scale bar = 20 μm. (A, B) shSTS-HaCaT or pcDNA3.1-STS HaCaT cells were used. (C, D) HaCaT cells were treated with STX-64 (0, 0.1, 1, and 10 μM) for 48 h. (E) pcDNA3.1-STS HaCaT cells were treated with STX-64 (0 and 10 μM) for 48 h. (G) Real-time qPCR was performed to detect the expression of E-cadherin, N-cadherin, and vimentin mRNA in shSTS-HaCaT and pcDNA3.1-STS HaCaT cells. Each data point represents the mean ± SEM of three experiments. *$p <$ 0.05 compared to control. (H) shSTS-HaCaT or pcDNA3.1-STS HaCaT cells were transfected with an E-cadherin promoter vector for 48 h. The relative firefly luciferase activity, normalized by the renilla luciferase activity, is shown. Each data point represents the mean ± SEM of three experiments. *$p < 0.05$ compared to control. (I) Chromatin immunoprecipitation (ChIP) assay on the E-cadherin promoter in shSTS-HaCaT or pcDNA3.1-STS HaCaT cells. Twist1 and c-Myc antibodies were used for the ChIP assay. Each data point represents the mean ± SEM of three experiments. *$p < 0.05$ compared to control.

of the Hippo pathway and suppression of HIF-1α expression.

3.4. STS modulates cellular respiration in HaCaT cells

Previous studies have reported that cellular respiration regulates the expression of HIF-1α and PHDs [16–18]. Based on the data in Fig. 2C, which suggests a potential role for STS in regulating cellular respiration, we further investigated how changes in STS expression affect mitochondrial respiration. Surprisingly, the results from extracellular flux oxygen consumption rate measurements revealed that cells transfected with STS-shRNA exhibited an approximately 2.6-fold increase in oxygen consumption rate (OCR) (Fig. 5A). This increase corresponded to a nearly 2.7-fold increase in ATP production (Fig. 5B). We also observed higher OCR rates in terms of basal respiration, maximal respiratory capacity, spare respiratory capacity, non-mitochondrial oxygen consumption, coupling efficiency (%), and spare respiratory capacity (%), thus confirming an overall increase in cellular respiration (Fig. 5B, C). Conversely, transient overexpression of STS in cells significantly

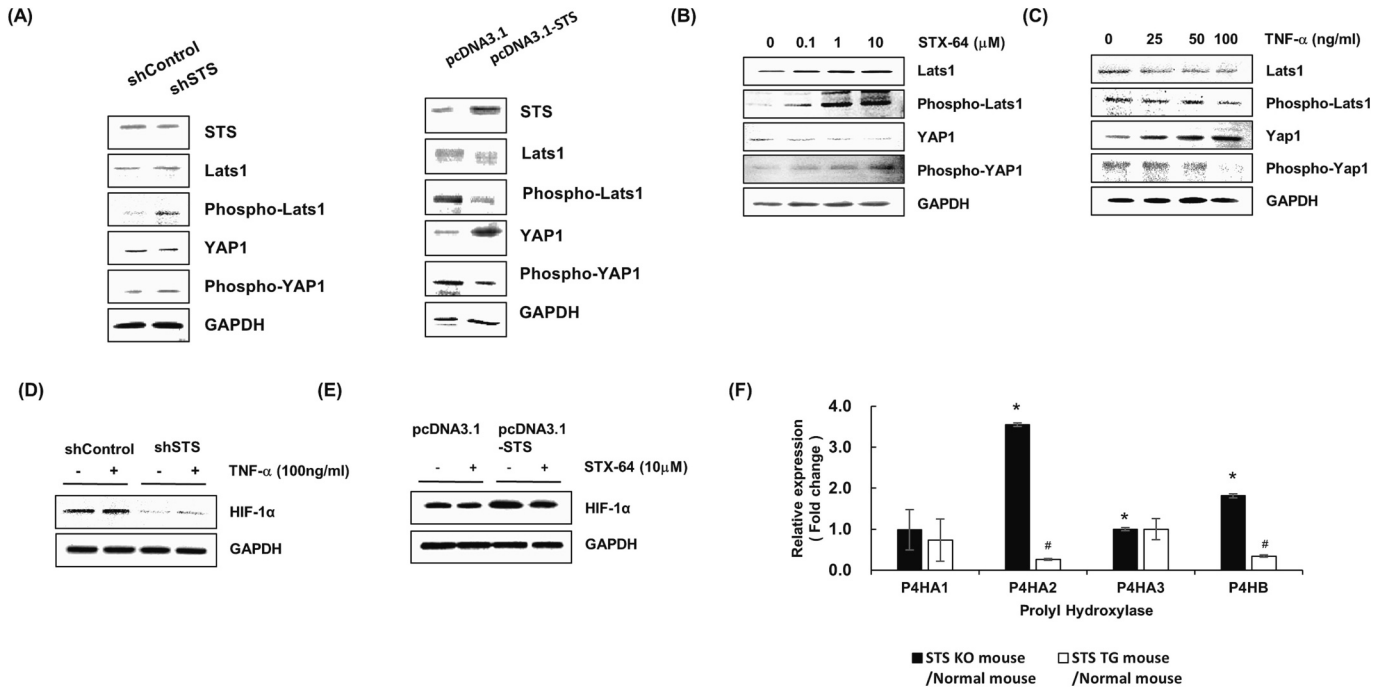

Fig. 4. STS deficiency increases Lats1 and suppresses YAP1 and HIF-1α expression. (A-C) Total cellular protein (20 μg) was subjected to western blot analysis using Lats1, phospho-Lats1, YAP1, and phospho-YAP1 antibodies. GAPDH was used as a loading control. (A) The experiments were conducted using shSTS-HaCaT or pcDNA3.1-STS HaCaT cells. (B) HaCaT cells were treated with STX-64 (0, 0.1, 1, and 10 μM) for 48 h. (C) HaCaT cells were treated with TNF-α (0, 25, 50, and 100 ng/ml) for 48 h. (D-E) Total cellular protein (20 μg) was subjected to western blot analysis using HIF-1α antibodies. GAPDH was used as a loading control. (D) shSTS-HaCaT cells were treated with TNF-α (0 and 100 ng/ml) for 48 h. (E) pcDNA3.1-STS HaCaT cells were treated with STX-64 (0 and 10 μM) for 48 h. (F) RNA-seq analysis of gene expression of prolyl hydroxylases. The data represent the mean ± SD (n = 3). $^{*,\ \#}p < 0.05$.

reduced OCR by approximately 4-fold and ATP production by approximately 3-fold (Fig. 5A, B), resulting in a hypoxic state. Furthermore, we depicted the energy map of STS knocked-down or overexpressed cells based on OCR and extracellular acidification rate (ECAR), thus demonstrating that cells tend to be more active and energetic when STS is deficient (Fig. 5D). These findings indicate that STS deficiency is closely involved in the induction of cellular respiration and energy metabolism.

Based on the metabolic analyses of cells following STS regulation, we determined the changes in gene expression related to mitochondrial function using our RNA-seq data to explore the detailed correlation between STS and cellular respiration. Interestingly, gene heatmaps and GSEA data revealed a significant induction of numerous genes associated with mitochondrial energy metabolism, oxidative stress, and oxidative phosphorylation in STS-deficient mice compared to STS TG mice, indicating a positive correlation between STS deficiency and activation of mitochondrial functions for cellular respiration (Fig. 5E, F, Supplementary Table S2).

Furthermore, key factors known to enhance mitochondrial respiratory functions, such as mitochondrial DNAs (mtDNAs), cytochrome *c* oxidases, and AMP-activated protein kinases (AMPKs), were substantially upregulated in STS-deficient mice compared to their STS-overexpressed counterparts (Fig. 5G) [45–47]. Importantly, all mtDNAs exhibited significant upregulation, ranging from a minimum of 1.2-fold to a maximum of 19-fold. Additionally, we assessed the level of intracellular ROS production, an important indicator of mitochondrial respiratory activation, following STS partial knockout using the CRISPR/Cas9 system or lentiviral overexpression of STS in HaCaT cells. Our findings demonstrated that STS deficiency caused a 2.6-fold increase in intracellular ROS production, whereas STS overexpression slightly inhibited ROS production (Fig. 5H). Collectively, our findings demonstrate that STS deficiency enhances mitochondrial respiration in human keratinocytes through the induction of mtDNAs, cytochrome *c* oxidases, and AMPKs, resulting in the establishment of a hyperoxic environment by promoting ROS generation.

3.5. STS deficiency increases ROS production, leading to the release of cytochrome c and modulation of gene expression associated with apoptosis

Previous studies have reported that increased ROS in keratinocytes can induce apoptosis [29,30]. Given that increased cell apoptosis in keratinocytes has been suggested as a cause of excessive stratum corneum formation, we investigated whether high levels of ROS in STS-deficient conditions induce apoptosis in keratinocytes, contributing to the symptoms of XLI. RNA-seq data showed a strong increase in the expression levels of genes associated with cell death and apoptosis in the absence of STS (Fig. 6A, B, Supplementary Table S3). Specifically, genes involved in mitochondrial permeabilization, a critical process for the release of cytochrome *c* from mitochondria to induce cell apoptosis, were significantly upregulated in STS KO mice compared to STS TG mice (Fig. 6C). Additionally, pro-apoptotic genes such as cytochrome *c*, Bax, Bak, Binp3, and Pmaip1 were significantly elevated, whereas the expression of the anti-apoptotic factor Bcl-xL was greatly decreased by STS deficiency in mice (Fig. 6D). Therefore, we concluded that STS deficiency in mice may induce intrinsic apoptosis by promoting cytochrome *c* release from mitochondria through the regulation of genes involved in mitochondrial permeabilization [30,48]. Additionally, we demonstrate that cells deficient in STS exhibit increased expression of the monomer and dimer form of Bnip3, which promotes increased cell membrane permeability (Fig. S3A, B).

To investigate whether STS deficiency promotes cytochrome *c* release from mitochondria, we measured the protein levels of cytochrome *c* in the cytosolic and mitochondrial fractions of STS partially knocked-out or stably STS-overexpressed cells. Consistent with the RNA-seq data, Bax and Bak, key factors for mitochondrial permeability, were translocated from the cytosol to mitochondria, which coincided with an increased release of cytochrome *c* from mitochondria to the cytosol in STS-deficient conditions. This suggests that translocated Bax and Bak

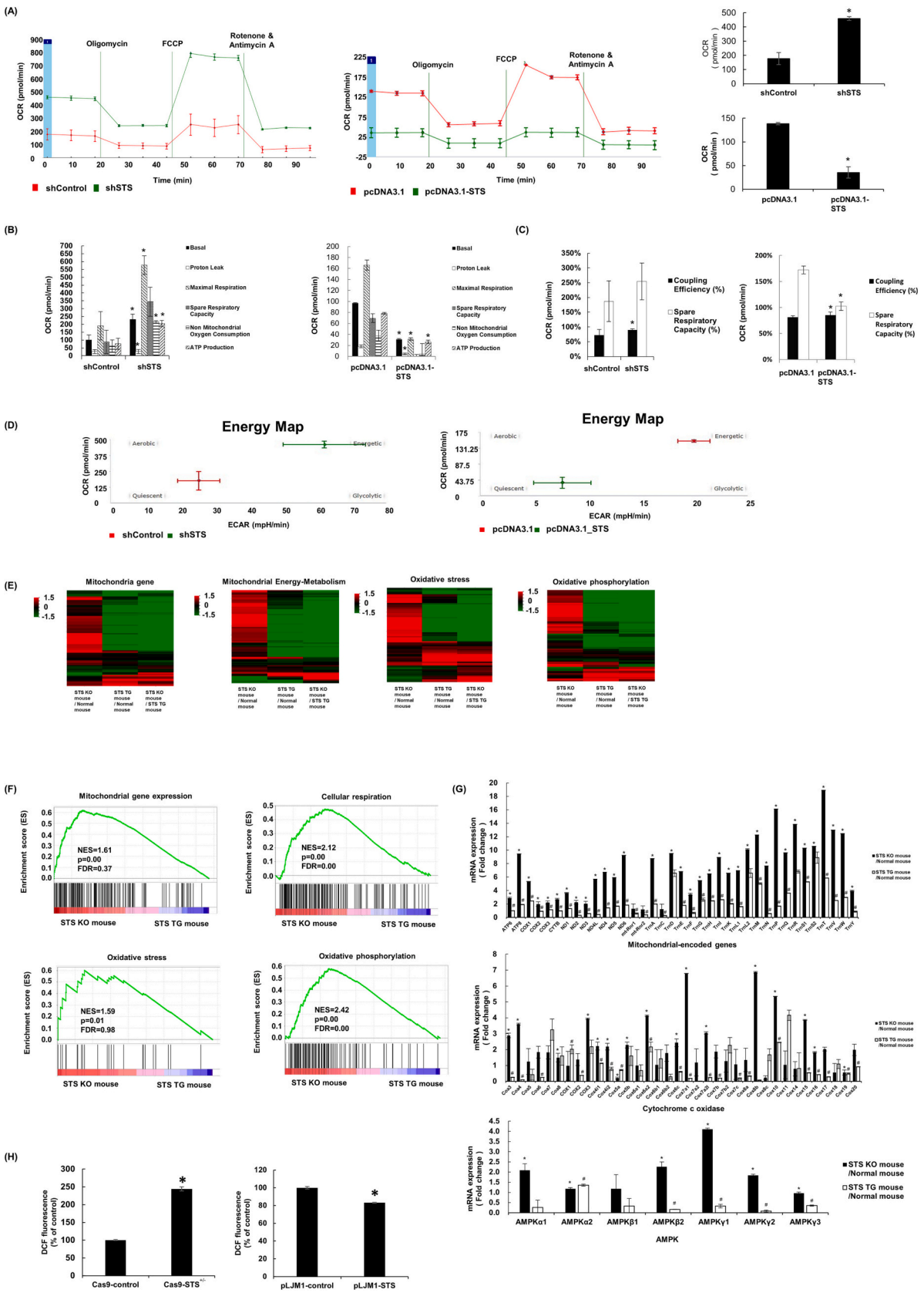

(caption on next page)

Fig. 5. STS deficiency increases cellular respiration and generates ROS. (A-D) Mitochondrial activity in shSTS-HaCaT or pcDNA3.1-STS HaCaT cells was determined by measuring the oxygen consumption rate (OCR) using the Seahorse Bioscience analyzer. OCR values for basal respiration, maximal respiration, ATP-coupled respiration, spare capacity, proton leak, and non-mitochondrial respiration were recorded and calculated. OCR was measured with serial injections of oligomycin (1 μM), FCCP (1 μM), antimycin (0.5 μM), and rotenone (0.5 μM). Each data point represents the mean ± SEM of three experiments. $*p < 0.05$ compared with control. (A) OCR. (B) Basal respiration, proton leak, maximal respiration, spare respiratory capacity, non-mitochondrial oxygen consumption, and ATP production. (C) Coupling efficiency (%) and spare respiratory capacity (%). (D) Energy map. (E) Heatmap analysis was performed on differentially expressed genes in each comparison group, and the expression was normalized and adjusted on a $\log_2$ scale. Red indicates upregulation, and green indicates downregulation. Heatmaps of mitochondrial genes, mitochondrial energy metabolism, oxidative stress, and oxidative phosphorylation in STS KO and STS TG mouse skin. (F) Mitochondrial gene expression, cellular respiration, oxidative stress, and oxidative phosphorylation pathways significantly enriched in STS KO and STS TG mouse skin by GSEA analysis. (G) RNA-seq analysis of gene expression in mtDNA, cytochrome *c* oxidase, and AMPK. The data represent the mean ± SD (n = 3). $^{*,\#}p < 0.05$. (H) ROS generation in Cas9-STS$^{+/-}$ and pLjm1-STS HaCaT cells were measured using 10 μM DCFH-DA, and fluorescence intensity was determined. Each data point represents the mean ± SEM of three experiments. $*p < 0.05$ compared with control. (For interpretation of the references to colour in this figure legend, the reader is referred to the web version of this article.)

may promote mitochondrial permeabilization by forming pores to release cytochrome *c* (Fig. 6E). Stably STS-overexpressing cells showed the opposite results (Fig. 6F). Additionally, we further investigated whether the increased cytochrome *c* release in STS partially knocked-out cells was triggered by the elevated levels of ROS generated due to STS deficiency. To examine this, we assessed the translocation of cytochrome *c*, Bax, and Bak in the presence of *N*-acetylcysteine (NAC), a ROS scavenger. Interestingly, under STS deficiency, the induction of cytochrome *c* release and mitochondrial translocation of Bax and Bak were strongly inhibited by NAC, suggesting that increased ROS levels due to

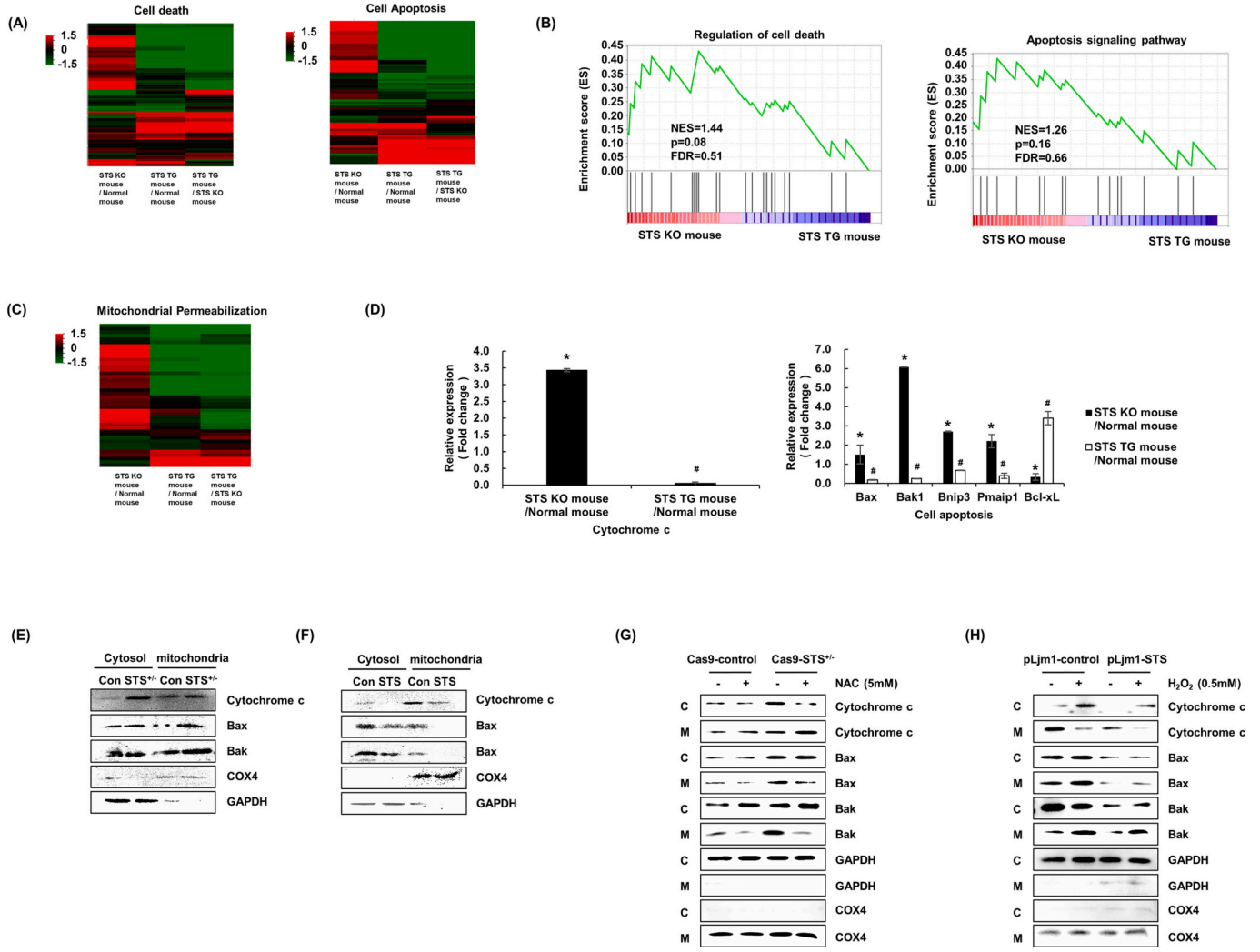

Fig. 6. STS deficiency induces cell apoptosis. (A, C) Heatmap analysis was performed on differentially expressed genes in each comparison group, and the expression was normalized and adjusted on a $\log_2$ scale. Red indicates upregulation, and green indicates downregulation. (A) Heatmaps of cell death and cell apoptosis in STS KO, STS TG, and normal mouse skin. (B) Significantly enriched regulation of cell death and apoptosis signaling pathways in STS KO and STS TG mouse skin by GSEA analysis. (C) Heatmaps of mitochondrial permeabilization in STS KO, STS TG, and normal mouse skin. (D) RNA-seq analysis of gene expression in cytochrome *c* and cell apoptosis factors. The data represent the mean ± SD (n = 3). $^{*,\#}p < 0.05$. (E, F, G, H) Mitochondrial and cytosolic lysates of cells were subjected to western blot analysis with cytochrome *c*, Bax, or Bak antibodies. (E) Cas9-STS$^{+/-}$ HaCaT cells were used. (F) pLjm1-STS HaCaT cells were used. (G) Cas9-STS$^{+/-}$ HaCaT cells were treated with NAC (5 mM) for 24 h. (H) pLjm1 HaCaT cells were treated with H_2O_2 (0.5 mM) for 24 h. (For interpretation of the references to colour in this figure legend, the reader is referred to the web version of this article.)

STS deficiency induce intrinsic apoptosis by promoting cytochrome *c* release (Fig. 6G). Conversely, ROS generation resulting from hydrogen peroxide (H_2O_2) in STS-overexpressing cells enhanced the induction of cytochrome *c* release and mitochondrial translocation of Bax and Bak (Fig. 6H).

Taken together, our findings demonstrate that higher ROS levels in STS-deficient conditions induce intrinsic apoptosis in human keratinocytes and skin tissues of mouse models by promoting the release of cytochrome *c* from mitochondria through the regulation of several genes involved in enhancing mitochondrial permeability. These findings shed light on the previously unknown mechanisms underlying the excessive formation of the stratum corneum in the skin of XLI patients.

4. Discussion

In this study, we investigated the impacts of STS deficiency on cell motility and apoptosis by examining gene expression in human keratinocyte cells (HaCaT) and skin tissues from newly generated STS KO and TG mouse models. Our in vivo experimental models for STS insufficiency provided valuable insights into the mechanisms underlying X-linked ichthyosis (XLI), thus complementing the findings of previous studies that were only capable of limited analysis, such as levels of metabolites or gene expression patterns in existing patient serum [31–33]. Moreover, RNA-seq analyses were conducted to examine the effects of STS on gene expression patterns associated with epithelial-mesenchymal transition (EMT) and mitochondrial apoptosis, which were previously difficult to study based solely on patient samples.

Interestingly, we found that STS deficiency downregulated the expression of HIF-1α, which is likely mediated by the upregulation of oxygen receptor PHD due to increased cellular respiration and ATP production in STS-insufficient conditions [16–18]. In addition to suppressing HIF-1α, a critical factor for EMT, STS deficiency activates the Hippo signaling pathway by regulating key genes, thus hindering cell mobility [15,49]. Recent studies have suggested a potential correlation between HIF-1α and the Hippo pathway, particularly the YAP/HIF-1α complex formation, which is activated during hypoxia. This complex binds to the PKM2 gene promoter and directly activate transcription, accelerating glycolysis under hypoxic conditions [50]. Further investigation is needed to determine if the downregulation of HIF-1α in STS deficiency can activate the Hippo signaling pathway.

Surprisingly, we found that STS deficiency significantly enhanced the signal pathway associated with mitochondrial respiration. Notably, there was a remarkable increase in the expression of mtDNA in the absence of STS. mtDNA is more susceptible to DNA damage compared to nuclear DNA due to the lack of protective histones, continuous exposure to ROS in the inner mitochondrial membrane, and limited DNA repair systems [45,51,52]. mtDNA is more likely to exhibit mutated forms, as mtDNA mutations occur 10–20 times more frequently than nuclear DNA mutations [51,52]. Therefore, increased mtDNA in STS deficiency may also result in mutations with a high probability. mtDNA mutations can cause mitochondrial dysfunction, and previous studies have reported 3- to 5-fold increases in mtDNA mutation levels due to cellular senescence, ROS formation, and apoptosis in a mouse mode [53,54]. These findings align with our results, indicating significant induction of mtDNA expression and ROS generation in STS deficiency, which activate Hippo signaling and promote mitochondrial apoptosis [54]. However, additional studies are needed to uncover the specific mechanism through which STS controls mtDNA expression.

Apoptosis is a programmed process that occurs during keratinocyte differentiation [20]. In our study, we found that STS deficiency caused cell cycle arrest in the G_0/G_1 phase, inhibiting cell proliferation and promoting keratinocyte differentiation (Fig. S1B-G). Our RNA-seq data supported these findings, revealing significant upregulation of keratin differentiation markers, such as keratin 1, keratin 10, and keratinocyte differentiation-associated protein (KRTdap) in response to STS depletion (Fig. S1G). These observations suggest that STS deficiency may enhance keratinocyte apoptosis by inducing cell differentiation.

Apoptosis in the epidermis is known to be activated by UVB radiation-induced cell damage, which increases ROS levels [8,23,24]. Our data demonstrates that STS deficiency also promotes ROS generation by enhancing mitochondrial respiration, leading to increased oxidative stress and activation of oxidative phosphorylation. This suggests that apoptosis may occur in the epidermis under STS-deficient conditions. Additionally, keratinocyte apoptosis, which is primarily observed in the basal layer of the epidermis, is an active, rapid, and energy-dependent process [55]. In STS-deficient conditions, human keratinocytes showed significantly elevated cellular energy levels (Fig. 5D), indicating that keratinocytes under STS-deficient conditions may undergo apoptosis. This excessive cell apoptosis is likely responsible for excessive stratum corneum formation in XLI.

Our analyses indicated that STS deficiency inhibits cell migration by suppressing the EMT process and promotes intrinsic cell apoptosis by enhancing mitochondrial respiration, which results in excessive ROS production in human keratinocytes and mouse skin tissues. Based on these findings, we proposed a novel molecular mechanism for the excessive formation of stratum corneum, thus expanding our understanding of the mechanisms that drive XLI. Although XLI remains an incurable disease, our findings may provide valuable insights for the development of new and effective therapeutic strategies.

Compliance with ethical standards

All animal experiments were approved by the Institutional Animal Care and Use Committee (IACUC) of Chung-Ang University (2017-00096, 2019-00003) and were performed according to the guidelines of an approved protocol by IACUC.

CRediT authorship contribution statement

Tae-Uk Kwon: Conceptualization, Data curation, Formal analysis, Investigation, Methodology, Writing – original draft, Writing – review & editing. **Yeo-Jung Kwon:** Supervision, Validation, Writing – review & editing. **Hyoung-Seok Baek:** Data curation, Formal analysis, Investigation. **Hyemin Park:** Investigation. **Hyein Lee:** Investigation. **Young-Jin Chun:** Conceptualization, Funding acquisition, Supervision, Validation, Writing – review & editing.

Declaration of competing interest

The authors declare no conflicts of interest.

Data availability

Data will be made available on request.

Acknowledgments

This study was supported by the National Research Foundation of Korea (NRF) funded by the Korean government (MSIP) (NRF-2021R1A2C201239513 and NRF-2022R1A5A600076012).

Appendix A. Supplementary data

Supplementary data to this article can be found online at https://doi.org/10.1016/j.bbadis.2023.167004.

References

[1] L.J. Shapiro, P. Yen, D. Pomerantz, E. Martin, L. Rolewic, T. Mohandas, Molecular studies of deletions at the human steroid sulfatase locus, Proc. Natl. Acad. Sci. U. S. A. 86 (1989) 8477–8481, https://doi.org/10.1073/pnas.86.21.8477.

[2] V. Ingordo, G. D'Andria, C. Gentile, M. Decuzzi, E. Mascia, L. Naldi, Frequency of X-linked ichthyosis in coastal southern Italy: a study on a representative sample of

a young male population, Dermatology 207 (2003) 148–150, https://doi.org/10.1159/000071784.
[3] G. Lykkesfeldt, A.E. Lykkesfeldt, N.E. Skakkebaek, Steroid sulphatase in man: a non inactivated X-locus with partial gene dosage compensation, Hum. Genet. 65 (1984) 355–357, https://doi.org/10.1007/BF00291559.
[4] C. Taraska, Ichthyosis, in: Brenner's Encyclopedia of Genetics, 2nd edition, 2013, pp. 1–4, https://doi.org/10.1016/B978-0-12-374984-0.00763-4.
[5] P.M. Elias, M.L. Williams, E.H. Choi, K.R. Feingold, Role of cholesterol sulfate in epidermal structure and function: lessons from X-linked ichthyosis, Biochim. Biophys. Acta 1841 (2014) 353–361, https://doi.org/10.1016/j.bbalip.2013.11.009.
[6] T.C. Wikramanayake, O. Stojadinovic, M. Tomic-Canic, Epidermal differentiation in barrier maintenance and wound healing, Adv. Wound Care (New Rochelle) 3 (2014) 272–280, https://doi.org/10.1089/wound.2013.0503.
[7] I. Pastar, et al., Epithelialization in wound healing: a comprehensive review, Adv. Wound Care (New Rochelle) 3 (2014) 445–464, https://doi.org/10.1089/wound.2013.0473.
[8] T. Geiger, H. Sabanay, N. Kravchenko-Balasha, B. Geiger, A. Levitzki, Anomalous features of EMT during keratinocyte transformation, PloS One 3 (2008) e1574, https://doi.org/10.1371/journal.pone.0001574.
[9] S.E. Leggett, A.M. Hruska, M. Guo, I.Y. Wong, The epithelial-mesenchymal transition and the cytoskeleton in bioengineered systems, Cell Commun. Signal 19 (2021) 32, https://doi.org/10.1186/s12964-021-00713-2.
[10] G. Barriere, P. Fici, G. Gallerani, F. Fabbri, M. Rigaud, Epithelial mesenchymal transition: a double-edged sword, Clin. Transl. Med. 4 (2015) 14, https://doi.org/10.1186/s40169-015-0055-4.
[11] J.P. Thiery, Epithelial-mesenchymal transitions in tumour progression, Nat. Rev. Cancer 2 (2002) 442–454, https://doi.org/10.1038/nrc822.
[12] J.M. Lee, S. Dedhar, R. Kalluri, E.W. Thompson, The epithelial-mesenchymal transition: new insights in signaling, development, and disease, J. Cell Biol. 172 (2006) 973–981, https://doi.org/10.1083/jcb.200601018.
[13] G.L. Semenza, Targeting HIF-1 for cancer therapy, Nat. Rev. Cancer 3 (2003) 721–732, https://doi.org/10.1038/nrc1187.
[14] W.K. Kim, et al., β-Catenin activation down-regulates cell-cell junction-related genes and induces epithelial-to-mesenchymal transition in colorectal cancers, Sci. Rep. 9 (2019) 18440, https://doi.org/10.1038/s41598-019-54890-9.
[15] I. Akrida, V. Bravou, H. Papadaki, The deadly cross-talk between hippo pathway and epithelial-mesenchymal transition (EMT) in cancer, Mol. Biol. Rep. 49 (2022) 10065–10076, https://doi.org/10.1007/s11033-022-07590-z.
[16] G.L. Semenza, HIF-1, O-2, and the 3 PHDs: how animal cells signal hypoxia to the nucleus, Cell 107 (2001) 1–3, https://doi.org/10.1016/s0092-8674(01)00518-9.
[17] K. Hirota, HIF-α prolyl hydroxylase inhibitors and their implications for biomedicine: a comprehensive review, Biomedicines 9 (2021) 468, https://doi.org/10.3390/biomedicines9050468.
[18] T.L. Nguyen, R.V. Duran, Prolyl hydroxylase domain enzymes and their role in cell signaling and cancer metabolism, Int. J. Biochem. Cell B. 80 (2016) 71–80, https://doi.org/10.1016/j.biocel.2016.09.026.
[19] S. Shin, et al., Human steroid sulfatase induces Wnt/β -catenin signaling and epithelial-mesenchymal transition by upregulating Twist1 and HIF-1α in human prostate and cervical cancer cells, Oncotarget 8 (2017) 61604–61617, https://doi.org/10.18632/oncotarget.18645.
[20] D. Raj, D.E. Brash, D. Grossman, Keratinocyte apoptosis in epidermal development and disease, J. Invest. Dermatol. 126 (2006) 243–257, https://doi.org/10.1038/sj.jid.5700008.
[21] S. Lippens, G. Denecker, P. Ovaere, P. Vandenabeele, W. Declercq, Death penalty for keratinocytes: apoptosis versus cornification, Cell Death Differ. 12 (Suppl. 2) (2005) 1497–1508, https://doi.org/10.1038/sj.cdd.4401722.
[22] S. Salucci, S. Burattini, M. Battistelli, V. Baldassarri, M.C. Maltarello, E. Falcieri, Ultraviolet B (UVB) irradiation-induced apoptosis in various cell lineages in vitro, Int. J. Mol. Sci. 14 (2013) 532–546, https://doi.org/10.3390/ijms14010532.
[23] D.E. Heck, A.M. Vetrano, T.M. Mariano, J.D. Laskin, UVB light stimulates production of reactive oxygen species: unexpected role for catalase, J. Biol. Chem. 278 (2003) 22432–22436, https://doi.org/10.1074/jbc.C300048200.
[24] T. Bito, C. Nishigori, Impact of reactive oxygen species on keratinocyte signaling pathways, J. Dermatol. Sci. 68 (2012) 3–8, https://doi.org/10.1016/j.jdermsci.2012.06.006.
[25] M. Redza-Dutordoir, D.A. Averill-Bates, Activation of apoptosis signalling pathways by reactive oxygen species, Biochim. Biophys. Acta 1863 (2016) 2977–2992, https://doi.org/10.1016/j.bbamcr.2016.09.012.
[26] J.F. Turrens, Mitochondrial formation of reactive oxygen species, J. Physiol. 552 (2003) 335–344, https://doi.org/10.1113/jphysiol.2003.049478.
[27] M. Schieber, N.S. Chandel, ROS function in redox signaling and oxidative stress, Curr. Biol. 24 (2014) R453–R462, https://doi.org/10.1016/j.cub.2014.03.034.
[28] D.F. Wilson, Oxidative phosphorylation: regulation and role in cellular and tissue metabolism, J. Physiol. 595 (2017) 7023–7038, https://doi.org/10.1113/JP273839.
[29] D.B. Zorov, M. Juhaszova, S.J. Sollott, Mitochondrial reactive oxygen species (ROS) and ROS-induced ROS release, Physiol. Rev. 94 (2014) 909–950, https://doi.org/10.1152/physrev.00026.2013.
[30] C. Garcia-Perez, S.S. Roy, S. Naghdi, X. Lin, E. Davies, G. Hajnoczky, Bid-induced mitochondrial membrane permeabilization waves propagated by local reactive oxygen species (ROS) signaling, Proc. Natl. Acad. Sci. U. S. A. 109 (2012) 4497–4502, https://doi.org/10.1073/pnas.1118244109.
[31] S. Trent, et al., Steroid sulfatase-deficient mice exhibit endophenotypes relevant to attention deficit hyperactivity disorder, Psychoneuroendocrinology 37 (2012) 221–229, https://doi.org/10.1016/j.psyneuen.2011.06.006.
[32] J. Idkowiak, et al., Steroid sulfatase deficiency and androgen activation before and after puberty, J. Clin. Endocrinol. Metab. 101 (2016) 2545–2553, https://doi.org/10.1210/jc.2015-4101.
[33] Y. Song, et al., Genetic analysis of a 12-year-old boy with X-linked ichthyosis in association with sclerosing glomerulonephritis, Mol. Med. Rep. 8 (2013) 1183–1187, https://doi.org/10.3892/mmr.2013.1625.
[34] S.A. Stewart, et al., Lentivirus-delivered stable gene silencing by RNAi in primary cells, RNA 9 (2003) 493–501, https://doi.org/10.1261/rna.2192803.
[35] C. Pulido-Quetglas, et al., Scalable design of paired CRISPR guide RNAs for genomic deletion, PLoS Comput. Biol. 13 (2017) e1005341, https://doi.org/10.1371/journal.pcbi.1005341.
[36] A. Subramanian, et al., Gene set enrichment analysis: a knowledge-based approach for interpreting genome-wide expression profiles, Proc. Natl. Acad. Sci. U. S. A. 102 (2005) 15545–15550, https://doi.org/10.1073/pnas.0506580102.
[37] M.J. Reed, A. Purohit, L.W.L. Woo, S.P. Newman, B.V.L. Potter, Steroid sulfatase: molecular biology, regulation, and inhibition, Endocr. Rev. 26 (2005) 171–202, https://doi.org/10.1210/er.2004-0003.
[38] B.Y. Suh, et al., Induction of steroid sulfatase expression by tumor necrosis factor-alpha through phosphatidylinositol 3-kinase/Akt signaling pathway in PC-3 human prostate cancer cells, Exp. Mol. Med. 43 (2011) 646–652, https://doi.org/10.3858/emm.2011.43.11.073.
[39] P. Nussbaumer, A. Billich, Steroid sulfatase inhibitors, Med. Res. Rev. 24 (2004) 529–576, https://doi.org/10.1002/med.20008.
[40] P.S. Pavithra, A. Mehta, R.S. Verma, Aromadendrene oxide 2, induces apoptosis in skin epidermoid cancer cells through ROS mediated mitochondrial pathway, Life Sci. 197 (2018) 19–29, https://doi.org/10.1016/j.lfs.2018.01.029.
[41] J. Jia, et al., Yes-associated protein promotes the abnormal proliferation of psoriatic keratinocytes via an amphiregulin dependent pathway, Sci. Rep. 8 (2018) 14513, https://doi.org/10.1038/s41598-018-32522-y.
[42] J. Yang, et al., Twist induces epithelial-mesenchymal transition and cell motility in breast cancer via ITGB1-FAK/ILK signaling axis and its associated downstream network, Int. J. Biochem. Cell Biol. 71 (2016) 62–71, https://doi.org/10.1016/j.biocel.2015.12.004.
[43] S. Yin, V.T. Cheryan, L. Xu, A.K. Rishi, K.B. Reddy, Myc mediates cancer stem-like cells and EMT changes in triple negative breast cancers cells, PloS One 12 (2017) e0183578, https://doi.org/10.1371/journal.pone.0183578.
[44] K.B. Cho, M.K. Cho, W.Y. Lee, K.W. Kang, Overexpression of c-myc induces epithelial mesenchymal transition in mammary epithelial cells, Cancer Lett. 293 (2010) 230–239, https://doi.org/10.1016/j.canlet.2010.01.013.
[45] C. Lawless, L. Greaves, A.K. Reeve, D.M. Turnbull, A.E. Vincent, The rise and rise of mitochondrial DNA mutations, Open Biol. 10 (2020) 200061, https://doi.org/10.1098/rsob.200061.
[46] B. Ludwig, E. Bender, S. Arnold, M. Huttemann, I. Lee, B. Kadenbach, Cytochrome C oxidase and the regulation of oxidative phosphorylation, Chembiochem 2 (2001) 392–403, https://doi.org/10.1002/1439-7633(20010601)2:6<392::AID-CBIC392>3.0.CO;2-N.
[47] X. Song, E. Tsakiridis, G.R. Steinberg, Y. Pei, Targeting AMP-activated protein kinase (AMPK) for treatment of autosomal dominant polycystic kidney disease, Cell. Signal. 73 (2020) 109704, https://doi.org/10.1016/j.cellsig.2020.109704.
[48] L. Galluzzi, O. Kepp, C. Trojel-Hansen, G. Kroemer, Mitochondrial control of cellular life, stress, and death, Circ. Res. 111 (2012) 1198–1207, https://doi.org/10.1161/CIRCRESAHA.112.268946.
[49] E. Rognoni, G. Walko, The roles of YAP/TAZ and the hippo pathway in healthy and diseased skin, Cells 8 (2019) 411, https://doi.org/10.3390/cells8050411.
[50] X. Zhang, et al., Yes-associated protein (YAP) binds to HIF-1α and sustains HIF-1α protein stability to promote hepatocellular carcinoma cell glycolysis under hypoxic stress, J. Exp. Clin. Cancer Res. 37 (2018) 216, https://doi.org/10.1186/s13046-018-0892-2.
[51] N.Z. Lax, D.M. Turnbull, A.K. Reeve, Mitochondrial mutations: newly discovered players in neuronal degeneration, Neuroscientist 17 (2011) 645–658.
[52] A. Konrad, et al., Mitochondrial mutation rate, spectrum and heteroplasmy in Caenorhabditis elegans spontaneous mutation accumulation lines of differing population size, Mol. Biol. Evol. 34 (2017) 1319–1334, https://doi.org/10.1177/1073858411385469.
[53] K. Ishikawa, ROS-generating mitochondrial DNA mutations can regulate tumor cell metastasis, Science 321 (2008) 342, https://doi.org/10.1126/science.1156906.
[54] A. Trifunovic, et al., Premature ageing in mice expressing defective mitochondrial DNA polymerase, Nature 429 (2004) 417–423, https://doi.org/10.1038/nature02517.
[55] E. Candi, R.A. Knight, E. Panatta, A. Smirnov, G. Melino, Cornification of the skin: a non-apoptotic cell death mechanism, in: Encyclopedia of Life Sciences, 2016, pp. 1–10, https://doi.org/10.1002/9780470015902.a0021583.pub2.